Patterns of CaCO$_3$ deposition in the eastern tropical Pacific Ocean for the last 150 kyr: Evidence for a southeast Pacific depositional spike during marine isotope stage (MIS) 2

Mitchell Lyle

Center for Geophysical Investigation of the Shallow Subsurface, Boise State University, Boise, Idaho, USA

Alan Mix and Nicklas Pisias

College of Ocean and Atmospheric Sciences, Oregon State University, Corvallis, Oregon, USA

[1] We constructed biogenic mass accumulation rate (MAR) time series for eastern Pacific core transects across the equator at ~105° and ~85°W and along the equator from 80° to 140°W. We used empirical orthogonal function (EOF) analysis to extract spatially coherent patterns of CaCO$_3$ deposition for the last 150 kyr. EOF mode 1 (51% variance) is a CaCO$_3$ MAR spike centered in marine oxygen isotope stage 2 (MIS 2) found under the South Equatorial Current. EOF mode 2 (19% of variance) is high north of the equator. EOF mode 3 (9% of variance) is an east-west mode centered along the North Equatorial Counter Current. The MIS 2 CaCO$_3$ spike is the largest event in the eastern Pacific for the last 150 kyr: CaCO$_3$ MARs are 2–3 times higher at 18 ka than elsewhere in the record, including MIS 6. It is caused by high CaCO$_3$ production rather than minimal dissolution. EOF 2, while it resembles deep water flow patterns, nevertheless, shows coherence to C$_{org}$ deposition and is probably also driven by CaCO$_3$ production. *INDEX TERMS:* 4267 Oceanography: General: Paleoceanography; 1615 Global Change: Biogeochemical processes (4805); 1030 Geochemistry: Geochemical cycles (0330); 3022 Marine Geology and Geophysics: Marine sediments—processes and transport; *KEYWORDS:* late Pleistocene, paleoproductivity, Pacific, calcite, biogeochemistry, carbon cycle

1. Introduction

[2] The cyclic pattern of CaCO$_3$ deposition is one of the first widely recognized climatic signals in deep-sea sediments [*Arrhenius*, 1952]. The origin of the CaCO$_3$ cycles has been hotly debated since their discovery, and it is still undecided whether the periodicity has been caused primarily by cyclic changes in deep ocean carbonate chemistry (dissolution) or by periodic changes in CaCO$_3$ production. In the Atlantic Ocean, where there is significant burial of terrestrial detritus, part of the signal could also be caused by variations in continental erosion. Evidence is strong that variability in both production and dissolution can strongly shape sedimentary CaCO$_3$ profiles and that either process could be a dominant factor regionally [*Broecker*, 1971; *Grötsch et al.*, 1991; *Berger*, 1992].

[3] Dilution by other phases can be assessed relatively easily by converting sedimentary time series to a burial flux, or mass accumulation rate (MAR), rather than attempting to interpret a time series of percentage data. It is more difficult to separate CaCO$_3$ production from dissolution in the sedimentary record. CaCO$_3$ MAR profiles can be compared to profiles of foraminiferan-based fragmentation or dissolution indices [*Berger*, 1971; *Berger et al.*, 1982], and these CaCO$_3$ MAR profiles can also be compared to other paleoproductivity indices [*Lyle et al.*, 1988; *Sarnthein et al.*, 1988; *Paytan et al.*, 1996].

[4] In this paper we will use EOF analysis upon a suite of eastern Pacific sediment cores (Figure 1 and Table 1) for additional insight into the formation of the carbonate record in the eastern equatorial Pacific. EOF analysis provides a means of eliciting spatially coherent end-member time series from a set of measurements at different locations. The regional distribution of the EOF modes as well as their temporal signal can provide important clues to the processes that caused them.

2. Oceanographic Setting

[5] Using spatial patterns to distinguish between production of CaCO$_3$ (a surface process) and dissolution (a deep process) requires a geographical sense of the important water flows and productivity centers in the eastern Pacific. Surface water processes in the tropics, because of the tradewinds, tend to be extended along lines of latitude except where the eastern boundary of the Pacific Ocean confines flow and changes wind directions (Figure 2a). In contrast, deep water processes find their expression shaped by the configuration of the eastern Pacific basins and by the typical flow path of Pacific Bottom Water (Figure 2b).

2.1. Surface Circulation

[6] The eastern tropical Pacific is marked by zonal currents and strong upwelling at the equator and in the easternmost Pacific (Figure 2a) [*Wyrtki*, 1974]. A fundamental feature of the zonal currents is their assymetry about the equator, caused by the northerly position of the Intertropical Convergence Zone (ITCZ). The westward flowing South Equatorial Current (SEC) is driven by the southeast trade winds. It extends from around 10°S to ~4°N across the equator. The North Equatorial Current (NEC) extends from ~8° to 20°N and is driven by the northeast trade winds. The North Equatorial Counter Current (NECC) flows eastward between the NEC and SEC carrying warm, nutrient-poor surface waters from the western equatorial Pacific region. It roughly marks the position of the ITCZ. Moderately high productivity is found all along the equator because of the upwelling of nutrients and is indicated by the enhanced C$_{org}$ MAR in modern sediments beneath the equator (Figure 2a) (*Lyle* [1992] and data from *Lyle et al.* [1995]). The
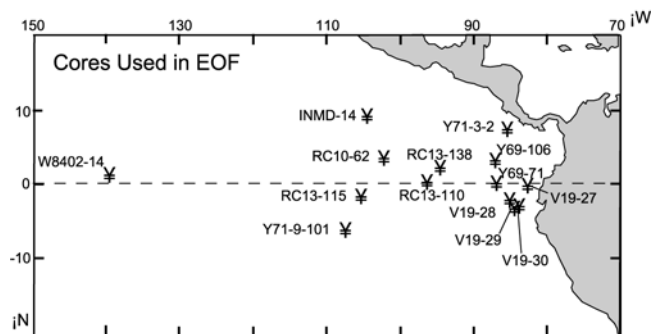
Figure 1. Location map of cores used in this study. See Table 1 for core locations and water depths.

Equatorial Undercurrent (EUC), an equatorially trapped subsurface current, flows from the western Pacific and partly balances the westward flow of equatorial surface waters.

[7] The eastern Pacific is also affected by eastern boundary currents. The Peru-Chile Current (PC), which brings waters of Antarctic origin toward the equator, is of the most importance to the eastern tropical Pacific. This flow, combined with upwelling along the coast of South America and the equator, produces a distinctive tongue of cold, nutrient-rich water which moves northward along the South American coast and turns westward along the equator. The cool waters are carried westward by the SEC which in turn can be distinguished by temperature. The California Current (CAC), the eastern boundary current of the subtropical North Pacific gyre, feeds subarctic waters into the northern tropics. Some of these waters are incorporated into the NEC.

2.2. Deep Water Circulation

[8] Pacific Bottom Water, a mixture of Antarctic Bottom Water, lower North Atlantic Deep Water, and some Antarctic Intermediate Water, flows into the Pacific in three tongues from the south. One tongue flows into the Tasman Basin (a dead end as far as the Pacific is concerned), and two flows enter the Pacific basin. The major flow travels along the western margin of the southwest Pacific, while a second flow enters the SE Pacific across the Chile Rise. Deep waters cross into the eastern Pacific basins over the East Pacific Rise from the west and the south [*Mantyla*, 1975; *Tsuchiya and Talley*, 1998] (Figure 2b). Between 10°N and 10°S this flow is primarily through fracture zone passages [*Mantyla*, 1975; *Lonsdale*, 1976] into both the Guatemala and Bauer Basins. Pacific Bottom Water which passes through fracture zones in the Chile Rise travels northward along the Peru-Chile Trench (Figure 2b). This water may also have an additional low-temperature, high-salinity component from the Ross Sea [*Gordon*, 1972].

[9] In the eastern Pacific basins, $CaCO_3$ dissolution is controlled by water properties inherited from Pacific deep water at the sill depth to each individual basin as well as local modification by C_{org} degradation and $CaCO_3$ dissolution in each basin. Because of these processes each basin has a distinct $CaCO_3$ compensation depth (CCD) [*Lyle et al.*, 1995].

3. Methods

[10] Cores used in this study are listed in Table 1 and are shown in Figure 1. Table 1 also lists the analyses for biogenic sediment components performed on each core. All cores have been analyzed for $CaCO_3$, and a subset has also been analyzed for C_{org} and opal, as listed in Table 1. All $CaCO_3$ and C_{org} analyses were performed at Oregon State University using the acidification/wet oxidation method described by *Weliky et al.* [1983] with modifications as by

Lyle et al. [1988]. Opal was analyzed by Na_2CO_3 digestion of the sediments and subsequent Si analysis either by atomic absorption spectrophotometry (cores INMD-14P, V19-28, W8402-14GC, Y71-3-2, and Y69-71 [*Lyle et al.*, 1988]) or by colorimetry (cores V19-27 and Y71-9-101 [*Mortlock and Froelich*, 1989]). Cores Y69-106 and V19-29 were analyzed for opal by the X-ray diffraction technique described by *Molina Cruz and Price* [1977], and the data are described in more detail by *Pisias* [1974] (Y69-106) and *Molina Cruz* [1976] (V19-29). Oxygen isotope analyses on benthic and planktonic foraminifera were performed in all cores and used for chronostratigraphy. We used existing oxygen isotope stratigraphy on cores V19-28, V19-29, and V19-30. Analyses for the other cores were completed at the Oregon State University Finnigan/MAT 251 automated mass spectrometer equipped with an Autoprep Systems carbonate preparation device. The analytic precision of $\delta^{18}O$ is better than 0.08‰. The isotopic time series were placed into a chronologic framework using the timescale of *Imbrie et al.* [1984].

4. Data

[11] Table A1 lists depth, age, dry bulk density, percentage of biogenic component, and oxygen isotope data for cores in this study.[1] The $CaCO_3$ data from each core, both weight percentage and MAR, were interpolated to 3 kyr spacing, and the 0–150 ka data are plotted in Figure 3, arranged with respect to the transects through the region.

4.1. Patterns of Sedimentary CaCO3 Weight Percent

[12] There is no simple dominant time series of $CaCO_3$ content for the eastern Pacific region (Figure 3). The only common pattern is a tendency for $CaCO_3$ to be lower in marine isotope stage (MIS) 5 (74–131 ka) than in other parts of the record. Only cores along the equator to the west of the Galapagos Islands (W8402-14, RC13-115, and RC13-110) have the ''classic'' Pacific $CaCO_3$ profile, which resembles an inverted oxygen isotope record. Cores within and just around the Panama Basin are also marked by a minimum at ~75 ka, which tends to be the lowest $CaCO_3$ interval in the entire 150 kyr period. Cores primarily from the southeastern quadrant of the study are marked by an additional $CaCO_3$ low between 40 and 50 ka (cores V19-28, V19-29, V19-30, and Y69-71). This $CaCO_3$ low also appears in INMD-1-14P. Clearly, there is a significant degree of structure either in $CaCO_3$ burial or in dilution by other sedimentary components within the eastern equatorial Pacific Ocean. To distinguish between the two alternatives, we examined MAR profiles which should remove dilution effects.

4.2. Patterns of CaCO3 Mass Accumulation Rate (MAR)

[13] The MAR is the burial flux of a sedimentary component in terms of mass per unit area per unit time. The calculation of MAR eliminates $CaCO_3$ peaks or troughs that are caused purely by changes in the relative rates of deposition of other sedimentary components (e.g., clays or opal) and also reveals flux changes when all components vary coherently with each other. It also removes the bias in percentage data which masks large flux changes at high percentages. For example, if noncarbonate deposition remains constant but burial flux of $CaCO_3$ in a sediment originally with 90% $CaCO_3$ is doubled, the $CaCO_3$ content only increases to 95%. The major flux change appears only as a minor percentage change.

[14] We calculated mass fluxes on the basis of dry bulk density estimated from $CaCO_3$ percent using the equation of *Murray* [1987] and using oxygen isotope stratigraphy to construct age

---

[1] Supporting Table A1 is available electronically at World Data Center-A for Paleoclimatology, NOAA/NGDC, 325 Broadway, Boulder, CO 80303, USA (email: paleo@mail.ngdc.noaa.gov; URL: http://www.ngdc.noaa.gov/paleo).

Table 1. Sediment Cores Used in this Study

Core Name	Latitude, °N	Longitude, °W	Water Depth, mbsl	Average Sedimentation Rate 0–150 ka, cm/kyr	Chemical Analyses
W8402A-14G	0.95	138.95	4287	1.5	CaCO$_3$, C$_{org}$, opal
INMD-14P	8.80	103.99	3135	2.0	CaCO$_3$, C$_{org}$, opal
RC10-62	3.33	101.72	3120	1.1	CaCO$_3$, C$_{org}$
RC13-115	−1.63	104.83	3621	1.7	CaCO$_3$, C$_{org}$
Y71-9-101	−6.38	106.94	3175	2.2	CaCO$_3$, C$_{org}$, opal
RC13-138	1.82	94.13	2655	4.9	CaCO$_3$
RC13-110	0.10	95.65	3231	2.3	CaCO$_3$
Y71-3-2	7.17	85.15	2164	3.0	CaCO$_3$, C$_{org}$, opal
Y69-106	2.98	86.55	2870	2.0	CaCO$_3$, C$_{org}$, opal
Y69-71	0.10	86.48	2740	6.5	CaCO$_3$, C$_{org}$, opal
V19-27	−0.47	82.07	1373	2.5	CaCO$_3$, C$_{org}$, opal
V19-28	−2.37	84.65	2720	4.5	CaCO$_3$, C$_{org}$, opal
V19-29	−3.58	83.93	3157	6.6	CaCO$_3$, opal
V19-30	−3.38	83.52	3091	6.3	CaCO$_3$

models, as discussed earlier. The most prominent pattern in the data set (Figure 3) is a CaCO$_3$ MAR spike in MIS 2 found primarily in cores in the southeastern equatorial Pacific (V19-27, V19-28, V19-29, V19-30, Y69-71, Y71-9-101, and RC13-115). This pattern was masked in the compositional profiles because of the high sedimentation rate but not particularly high CaCO$_3$ contents of MIS 2. The CaCO$_3$ spike matches in time the well-known eastern Pacific C$_{org}$ productivity spike [*Pedersen*, 1983; *Lyle et al.*, 1988; *Pedersen et al.*, 1991]. We do not think that the spike is an artifact caused by poor age control because the majority of the cores with the MIS 2 CaCO$_3$ spike have high sedimentation rates (Table 1) and the oxygen isotope record is well resolved. In addition, MIS 2 is a very easily identified isotope stage, so a miscorrelation is unlikely.

[15] Another prominent pattern is high CaCO$_3$ MAR between 25 and 50 ka found in cores to the north and northwest of the Galapagos Islands (Y71-3-2, INMD-14, RC10-62, and RC13-138). These cores also exhibit high CaCO$_3$ MARs in isotope stage 6 (>131 ka), resulting for the most part from changes in sedimentary concentration, not sedimentation rate.
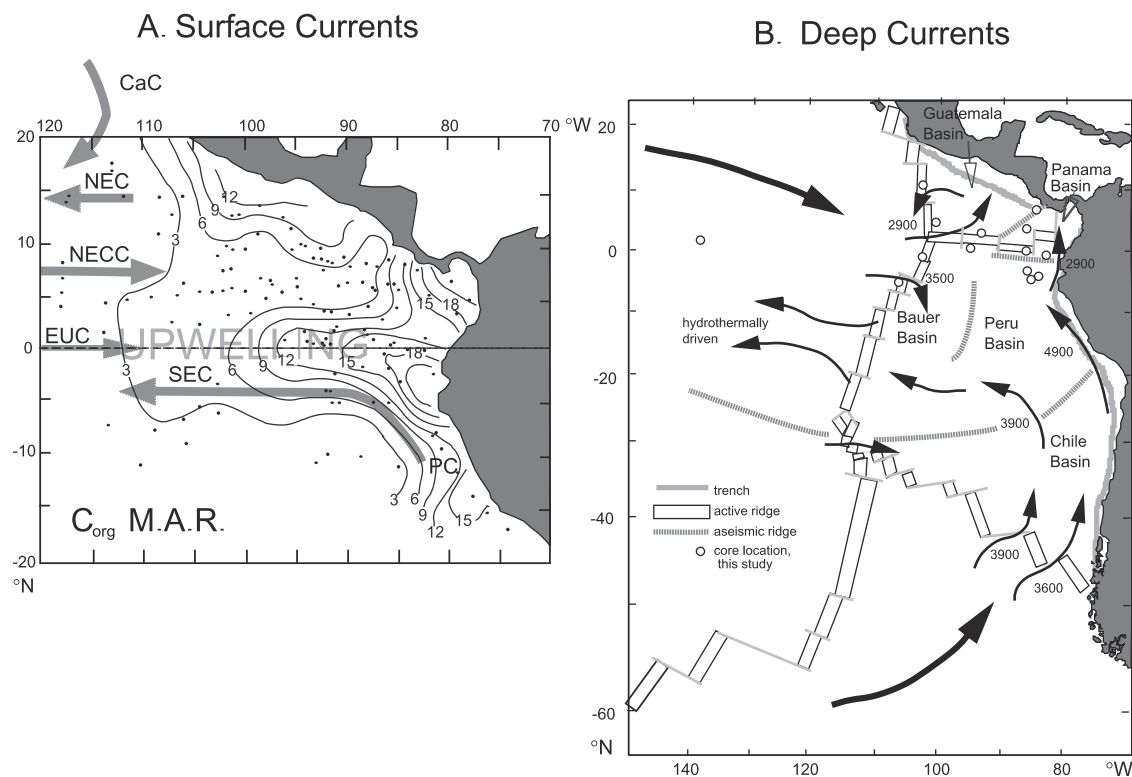

Figure 2. (a) Surface currents of the eastern tropical Pacific Ocean superimposed upon C$_{org}$ mass accumulation rate (MAR) from *Lyle* [1992]. C$_{org}$ MAR is a semiquantitative measure of productivity in the water column. CaC, California Current; EUC, Equatorial Undercurrent; NEC, North Equatorial Current; NECC, North Equatorial Countercurrent; SEC, South Equatorial Current. (b) Deep water flow paths in the eastern Pacific, based upon *Lonsdale* [1976] with additions from *Dymond* [1981] and *Lyle* [1992]. See color version of this figure at back of this issue.
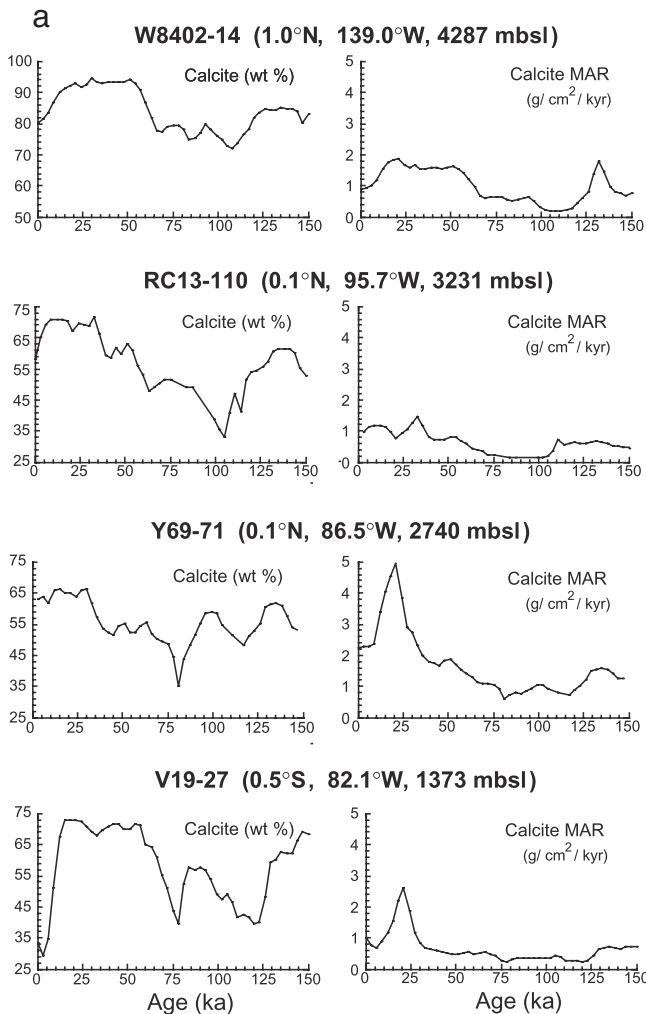
a

b

Figure 3. CaCO₃ weight percent and MAR time series for cores in this study, interpolated to 3 kyr spacing, 0–150 ka. (a) Equatorial transect from 82° to 139°W, (b) N-S transect at ~105°W, (c) N-S transect at ~85°W, and (d) Peru Basin depth transect, ~85°W.

[16] We observe no strong 100 kyr periodicity in either the CaCO₃ MAR or the CaCO₃ percent time series from eastern Pacific cores. While the 100 kyr cycle might be more prominent if we analyzed data for a time period longer than 150 kyr, the lack of strong low-order variance and the strength of shorter cycle periods (or events) is very much different from the CaCO₃ time series in the central Pacific Ocean [e.g., *Farrell and Prell*, 1989]. Compare, for example, the typical central Pacific core W8402-14 (Figure 3a) to the other CaCO₃ records in this study. The lack of similarity between eastern and central Pacific CaCO₃ time series has been previously noted on longer time series from the eastern Pacific [*Snoeckx and Rea*, 1994]. Unfortunately, few of the cores studied by *Snoeckx and Rea* [1994] have been dated using oxygen isotope stratigraphy; for the most part, we could not use them in this study.

5. Empirical Orthogonal Function (EOF) Analysis

[17] We applied EOF analysis to the eastern Pacific CaCO₃ MAR records through the last full glacial cycle (150–0 ka) to understand the spatial patterns of CaCO₃ deposition. This technique is used to reduce the time series into spatially coherent,

orthogonal eigenvectors. Each eigenvector represents an independent mode of variability within the data set, which can then be mapped geographically.

[18] More details about the technique are given by *Pisias and Mix* [1997]. Briefly, we used 3 kyr interpolated data and applied a time domain EOF technique to the time series from the 14 cores in the data set. A 14 × 14 correlation matrix was calculated from the 14 CaCO₃ MAR records and EOF were calculated by extracting eigenvalues and associated eigenvectors from this matrix. Three EOF were found to explain 80% of the variance in the CaCO₃ MAR data set (Tables 2 and 3).

[19] EOF 1 explained 51% of the total variance in the data set and is most highly loaded in cores from the southeastern Pacific (Figure 4). The EOF 1 time series is a CaCO₃ spike during MIS 2, with a maximum at 21 ka. The remainder of the time series, while muted, has a glacial-interglacial pattern with higher CaCO₃ MAR in the glacial periods. Cores with loadings >0.9 in this EOF occur primarily in the easternmost equatorial Pacific (cores Y69-71, V19-27, V19-28, V19-29, and V19-30), but Y71-9-101 on the East Pacific Rise also has very high loadings. The map pattern of EOF 1 is a tongue extending from the southeast Pacific along the equator, which drops off sharply in the north.

[20] EOF 2 is strongest in the northeastern tropical Pacific (Figure 5), and explains a further 19% of the variance in the data set. The EOF time series has strong power in the obliquity orbital
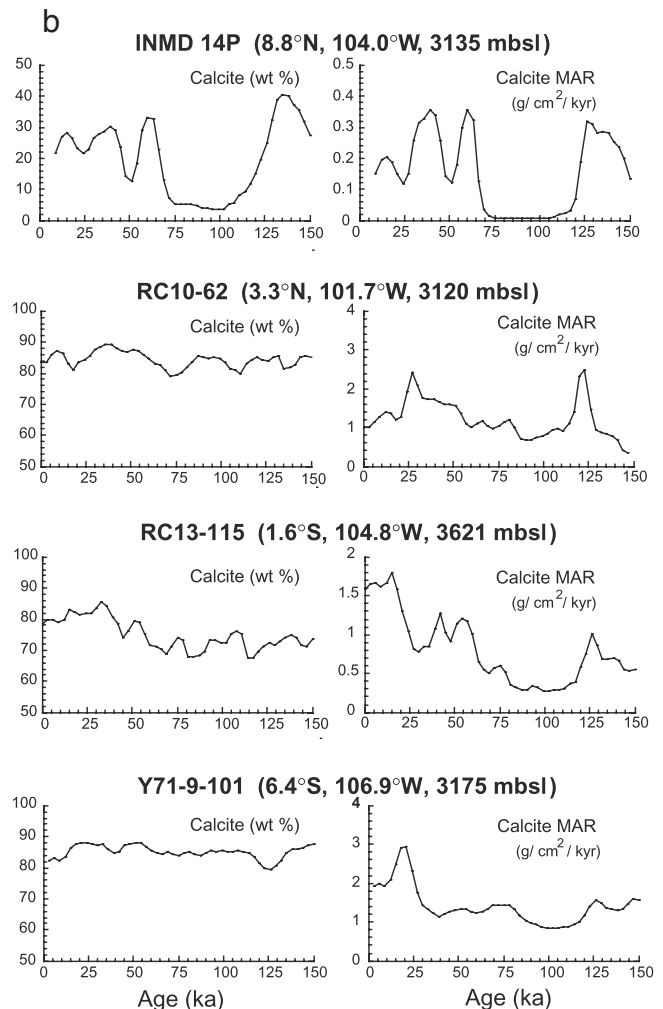
Figure 3.   (continued)

c

Y71-3-2 (7.2°N, 85.2°W, 2164 mbsl)

Y69-106 (3.0°N, 86.6°W, 2870 mbsl)

RC13-138 (1.8°N, 94.1°W, 2655 mbsl)

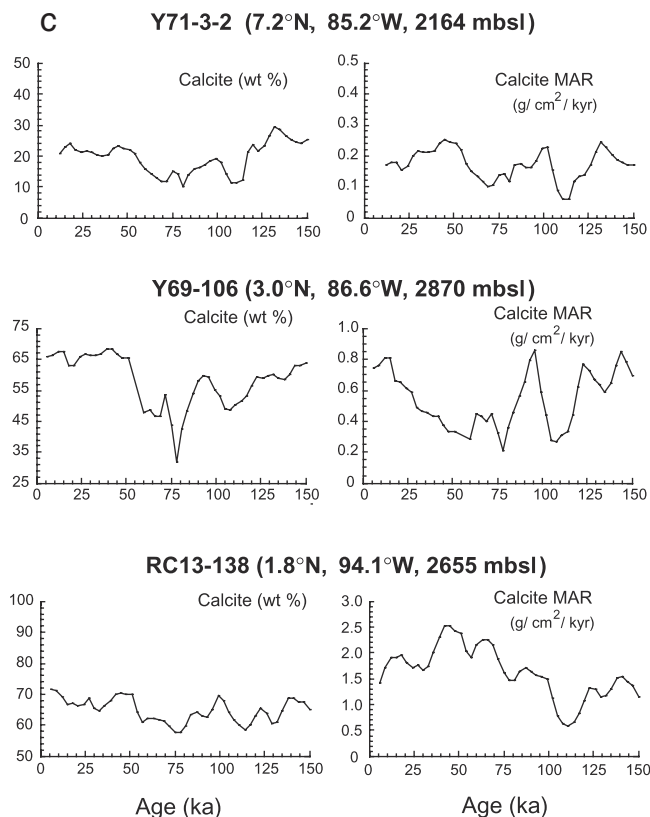Age (ka)   Age (ka)

Figure 3. (continued)

band (Figure 5). Cross-spectral analysis shows that the coherence between the orbital obliquity time series and EOF 2 is significant at >95% confidence interval, and the two signals are in phase. The CaCO₃ deposition represented by EOF 2 leads the obliquity component of regional sea surface temperature variability and ice volume [*Pisias and Mix*, 1997] because these signals slightly lag the orbital forcing. Cores with the highest loading of this EOF are located in the northeast of the survey region (cores INMD-14P and Y71-3-2).

[21] EOF 3 explains 9% of the variance in the data set and appears to be oriented east-west along the core of the NECC (Figure 6). The EOF has opposite sign for the Panama Basin and the remainder of the Pacific Ocean. EOF 3 is also coherent with the orbital obliquity time series at >95% confidence interval but leads obliquity by ~4–6 kyr. High positive loadings in EOF 3 are found only in core Y69-106, in the Panama Basin. High negative loadings are found in RC10-62, near the East Pacific Rise beneath the NECC.

6. Production or Deep Water Chemistry Controlling CaCO₃ EOF?

[22] On the basis of the following lines of evidence we conclude that CaCO₃ production not CaCO₃ dissolution is primarily responsible for the EOF patterns we observe.

1. The first is lack of similarity between eastern Pacific EOF and the central Pacific CCD time series of *Farrell and Prell* [1989]. The central Pacific time series should be more strongly controlled by deep water chemistry because the average water depth of the *Farrell and Prell* [1989] study is ~1.5 km deeper than in the eastern Pacific, and the pressure effect elevates the apparent solubility product constant for CaCO₃ by ~25% [*Pytkowicz*, 1969].

2. In a depth transect in the Peru Basin, highest dissolution and a shallow CCD coincide with highest CaCO₃ MAR, while the deepest CCD and lower dissolution coincide with a relatively low CaCO₃ MAR. This pattern can be best explained by a production-dominated signal.

3. Shallow sites within the same water mass around the Panama Basin have different time series. The best explanation is regional differences in CaCO₃ production.

4. The CaCO₃ MAR time series resemble those of C_{org} and biogenic opal MAR. The common behavior of each time series is best explained by changes in production.

5. The EOF map patterns cross basins or deepwater flow paths. They are more similar to the distribution of surface currents or surface water masses and are probably shaped by near-surface processes.

6.1. Comparisons Between the Eastern Pacific EOF and Central Pacific CCD

[23] The depth to the CCD is controlled by three separate fluxes: the rain rate of CaCO₃ from surface waters, the dissolution rate of CaCO₃ driven by undersaturation of bottom waters (deep water chemistry), and the dissolution rate of CaCO₃ coupled to the degradation of C_{org}. Of these three fluxes, two are production driven and should vary as a function of primary productivity. The third, undersaturation of bottom waters, should change on a global or basin-wide scale to reflect global changes in nutrient budgets or some redistribution of deep water flow paths [*Broecker and Takahashi*, 1978; *Broecker*, 1982].

[24] The central Pacific CCD record of *Farrell and Prell* [1989] should be a good reflection of the time series of calcite undersaturation in Pacific deep water. The sediment cores used to derive the record are located in a relatively stable oceanographic environment. All the sediment cores that define the lower lysocline and CCD (deeper than 4550 m below sea level (mbsl))
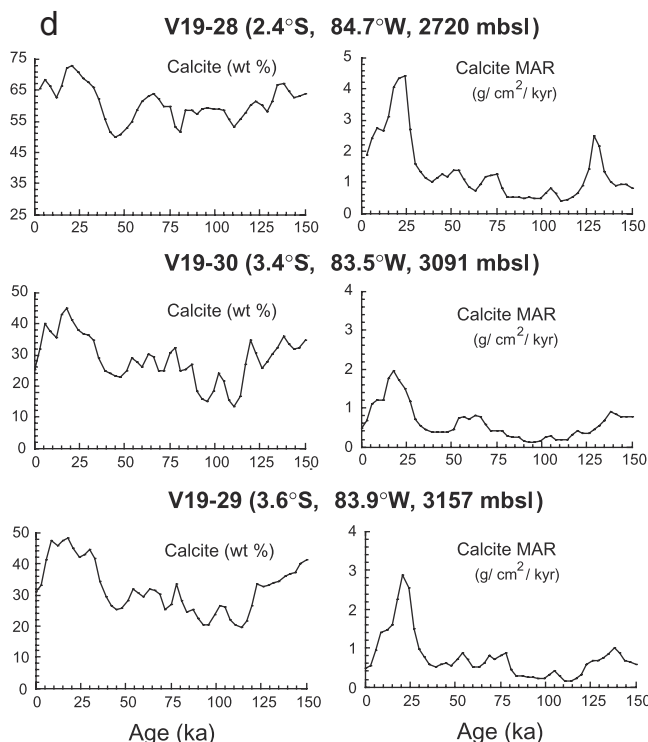
d

V19-28 (2.4°S, 84.7°W, 2720 mbsl)

V19-30 (3.4°S, 83.5°W, 3091 mbsl)

V19-29 (3.6°S, 83.9°W, 3157 mbsl)

Age (ka)   Age (ka)

Figure 3. (continued)

Table 2. Calcium Carbonate MAR EOF Time Series, Quartimax Rotation

Age, ka	EOF 1 Rotated Factor Score	EOF 2 Rotated Factor Score	EOF 3 Rotated Factor Score
0	0.1835	0.1247	0.1926
3	0.4971	0.0821	0.0959
6	0.9233	−0.0149	0.6600
9	1.2073	0.0456	0.4281
12	1.5273	0.2824	0.3545
15	2.1613	0.1361	0.5309
18	2.9205	−0.5534	0.3774
21	3.2832	−1.2813	0.2258
24	2.4987	−0.9566	−0.7549
27	1.1952	0.1170	−1.4061
30	0.4086	0.9444	−1.3379
33	0.0929	1.2937	−1.1299
36	−0.2080	1.4563	−1.0604
39	−0.3977	1.7164	−1.0115
42	−0.4078	1.9735	−0.8248
45	−0.4029	1.7305	−0.9646
48	−0.3791	1.2594	−1.1736
51	−0.1883	1.1912	−1.2410
54	0.0053	1.0261	−0.1958
57	−0.1211	0.8892	0.1511
60	−0.3865	0.7529	−0.6609
63	−0.3999	0.4126	−0.2066
66	−0.2683	−0.4398	−0.5158
69	−0.1864	−0.9601	−0.5777
72	−0.2657	−1.0751	−0.2421
75	−0.3537	−0.9879	−0.5490
78	−0.3949	−0.9120	−1.1847
81	−0.6012	−0.9558	−0.8702
84	−0.8807	−0.5374	0.1757
87	−0.9435	−0.4018	0.8320
90	−0.8730	−0.2639	0.8605
93	−0.8434	−0.1832	1.3116
96	−0.9009	−0.0397	1.5682
99	−1.1124	−0.1332	1.1014
102	−1.0141	−0.4566	0.6807
105	−0.8230	−1.3442	−0.2012
108	−0.6456	−1.8589	−0.6844
111	−0.7711	−1.8052	−0.7361
114	−0.6039	−1.8665	−0.8840
117	−0.7431	−1.1823	−0.5994
120	−0.5228	−0.6410	−1.0829
123	−0.3077	−0.1072	−0.7944
126	−0.1860	0.4035	0.5113
129	0.0107	0.6676	1.1532
132	−0.0657	0.9728	1.1767
135	−0.1433	0.7879	1.0627
138	−0.0929	0.4498	1.2535
141	−0.1536	0.2906	1.6962
144	−0.1871	0.1411	2.3332
147	−0.1398	−0.1894	2.1569
Variance explained in data set	51%	19%	9%

were recovered from latitudes between 2.5° and 6°N, outside the equatorial high productivity zone (~1°N–1°S).

[25] The record of upper lysocline changes, in contrast, probably has artifacts caused by changes in CaCO₃ production. Shallow cores in the depth transect tend to be from the equatorial region where CaCO₃ production and rain is highest and probably most variable on a glacial-interglacial scale [*Archer*, 1991]. The lower lysocline is defined by cores away from the equator where CaCO₃ rain is significantly less [*Honjo et al.*, 1995] and presumably varies to a lesser extent.

[26] The central Pacific CCD has a strong 100 kyr cyclicity, with a tendency within the last 300 kyr for the lowest CaCO₃ contents

and shallowest CCD to occur near the end of interglacial periods. The highest CaCO₃ contents and deepest CCD, in contrast, appear in the beginnings of the glacial periods. Nevertheless, the position of the CCD itself remained stable, within 100 m of its present position [*Farrell and Prell*, 1989], and the greatest changes occurred in the thickness of the lysocline.

[27] None of the three EOF time series we have extracted resemble the central Pacific CCD time series. In EOF 1 we observe a major CaCO₃ peak during MIS 2, and we have 41 kyr periodicity in EOF 2 and 3. While EOF 1 and 2 sum to a profile that is roughly a glacial-interglacial signal with high CaCO₃ in the glacial stages, in detail, it differs from the CCD time series. Highest CaCO₃ MARs, for example, occur in MIS 2 not in MIS 4 where the deepest central Pacific CCD occurs.

6.2. Peru Basin CCD

[28] We reconstruct the CCD time series in the northeastern Peru Basin using V19-28, V19-29, and V19-30 (Figures 3d and 7). They form a small depth transect that proves useful to investigate dissolution, the CCD, and the origin of the CaCO₃ EOF. All three cores, incidentally, have >0.9 loadings in EOF 1, the MIS 2 CaCO₃ spike. We observe (Figure 3d) that the deeper cores V19-29 and V19-30 have lower CaCO₃ percent and lower CaCO₃ MARs than V19-28 at every 3 kyr time slice, despite having higher sedimentation rates.

[29] The three time series appear to result from time-varying CaCO₃ rain with superimposed depth-dependent dissolution. We have constructed a simple model CCD (Figure 7) by using the rate of change of CaCO₃ MAR with depth to extrapolate to zero flux (i.e., the CCD) using either the difference between V19-30 (3091 m) and V19-28 (2720 mbsl) or V19-29 (3157 m) and V19-28. The result of this extrapolation is shown in the bottom graph of Figure 7, where the thick line is the depth to the CCD calculated by averaging smoothed estimates from V19-29 and V19-30. This "V19" model CCD is actually similar in shape to that from *Farrell and Prell* [1989] but is significantly shallower. The V19 CCD estimate is also shallower than estimates for the modern CCD in the Peru Basin (~4100 mbsl [*Lyle et al.*, 1995] and ~4200 mbsl [*Weber et al.*, 1995]). We suspect that a significant portion of the dissolution we observe could be caused by organic matter degradation in the high productivity northeastern corner of the Peru Basin. Alternatively, V19-28 (the shallow core) might lie in a region of slightly more sediment focusing than the deeper sites and thus exaggerate the change with depth.

[30] Because V19-28 is at or just above the lysocline in the Peru Basin [*Lyle et al.*, 1988], the CaCO₃ MAR at V19-28 approximates the CaCO₃ rain rate from the surface waters. The difference between the V19-28 CaCO₃ MAR and the V19-29 or V19-30 CaCO₃ MAR is an estimate of the rate of CaCO₃ dissolution from the seafloor in the upper lysocline of the Peru Basin. The time series of the rate of dissolution is similar in both sets of cores and is somewhat surprising (Figure 7). The highest rate of dissolution occurs during MIS 2 (12–24 ka), during the same interval with the highest CaCO₃ MAR, and when the CCD appears to be relatively flat. *Le et al.* [1995] also observed slightly higher fragmentation in forams during the MIS 2 interval in ODP Site 846, 6° to the west but nearly the same water depth as V19-29.

[31] Other time periods with relatively high dissolution are also periods of higher CaCO₃ MAR and relatively shallow CCD. The deep CCD intervals are actually marked by relatively low CaCO₃ MARs. This is precisely the pattern of CaCO₃ MAR expected from C$_{org}$-driven dissolution of CaCO₃ [*Berelson et al.*, 1994; *Jahnke et al.*, 1997] if the regional CaCO₃ rain through the water column does not increase as rapidly as the increased C$_{org}$ rain as productivity increases. An increase in C$_{org}$ rain relative to CaCO₃ during a primary productivity event causes higher dissolution of CaCO₃

Table 3. Calcium Carbonate MAR EOF Loadings

Core Name	Communality	EOF 1 Loading	EOF 2 Loading	EOF 3 Loading
W8402A-14GC	0.930	0.6519	0.6977	−0.1334
INMD-1-14P	0.683	0.2593	0.7838	0.0374
RC10-62	0.695	0.2808	0.2712	−0.7368
RC13-115	0.712	0.7193	0.4381	−0.0519
Y71-9-101	0.939	0.9670	0.0074	0.0599
RC13-138	0.508	0.2343	0.6337	−0.2280
RC13-110	0.616	0.6008	0.4480	−0.2329
Y71-3-2	0.736	0.0981	0.8340	0.1753
Y69-106	0.697	0.3843	0.1572	0.7245
Y69-71	0.948	0.9612	0.1311	−0.0818
V19-27	0.907	0.9478	0.0104	0.0935
V19-28	0.934	0.9640	0.0667	0.0122
V19-29	0.909	0.9536	−0.0057	−0.0021
V19-30	0.896	0.9383	0.0594	0.1123

through organic matter degradation even though the net burial of $CaCO_3$ might be higher than at other times.

[32] *Weber et al.* [1995] have independently estimated the late Neogene history of the CCD in the Peru Basin using sets of cores at ~90°W, from 6°30′ to 8°33′S and water depths of 3995–4245 m. These cores are deeper, 6° farther west, and at least 3° farther south than the V19 cores and sample through the western Peru Basin CCD. Although of coarse resolution, more carbonate appears in glacial stages and, of importance for this study, in MIS 2. *Weber et al.* [1995] also conclude that the CCD variations since ~400 ka are a result of higher $CaCO_3$ production in the Peru Current during glacials.

6.3. Shallow Sites Around the Panama Basin

[33] One would expect that cores at similar water depths within a water mass should have similar $CaCO_3$ time series if dissolution by changes in deep water chemistry is a strong control of $CaCO_3$

deposition. Three cores from the Panama Basin (Figure 8) are each highly loaded in a different EOF. They are all relatively close to each other (Figure 1), are all relatively shallow cores (between 2100 and 2900 mbsl), and should have experienced the same dissolution history since they are all from the Panama Basin. Nevertheless, they have radically different MAR time series. In addition, the shallowest but northernmost site of the three (Y71-3-2, 2164 mbsl) has the lowest average $CaCO_3$ MAR, while the core nearest the equator (Y69-71, 2740 mbsl), which should have experienced the greatest $CaCO_3$ production, has the highest average $CaCO_3$ MAR.

6.4. Comparisons Between $CaCO_3$, C_{org}, and Opal MAR

[34] The time series of opal, C_{org}, and $CaCO_3$ MAR all resemble each other in cores highly loaded in each of the three EOF (Figure 8). The three biogenic MAR delineate basically the same time series in each core: EOF 1 is marked by a biogenic
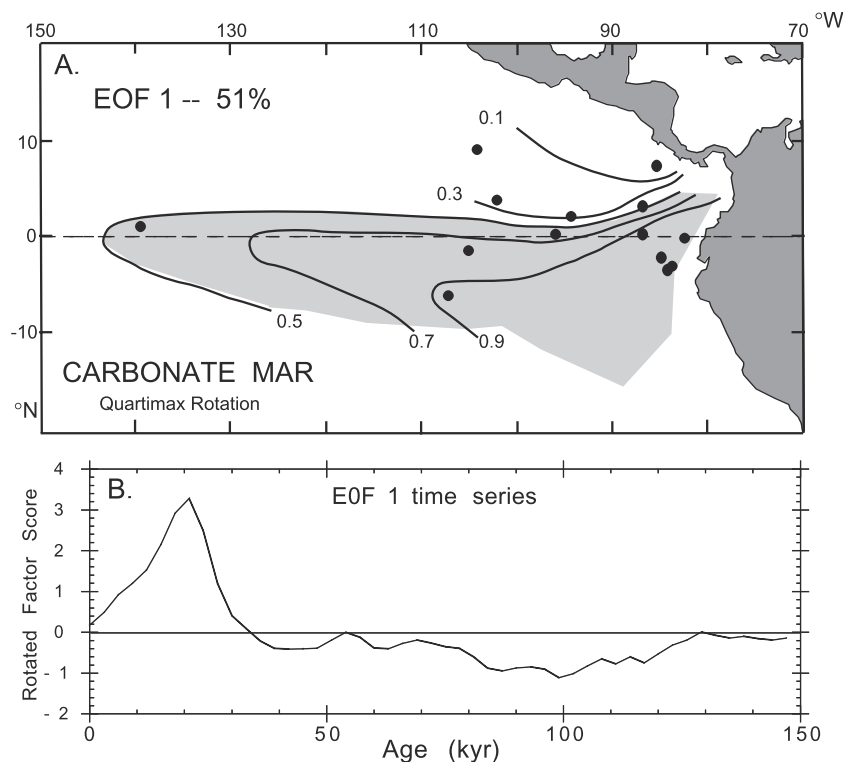

Figure 4. (a) Map pattern of factor loadings for EOF 1, which explains 51% of the variance in the $CaCO_3$ MAR data set. The pattern is reminiscent of the South Equatorial Current distriburion. (b) $CaCO_3$ MAR time series of EOF 1. The time series is marked by a strong MAR peak at 21 ka and a muted long-period variability.
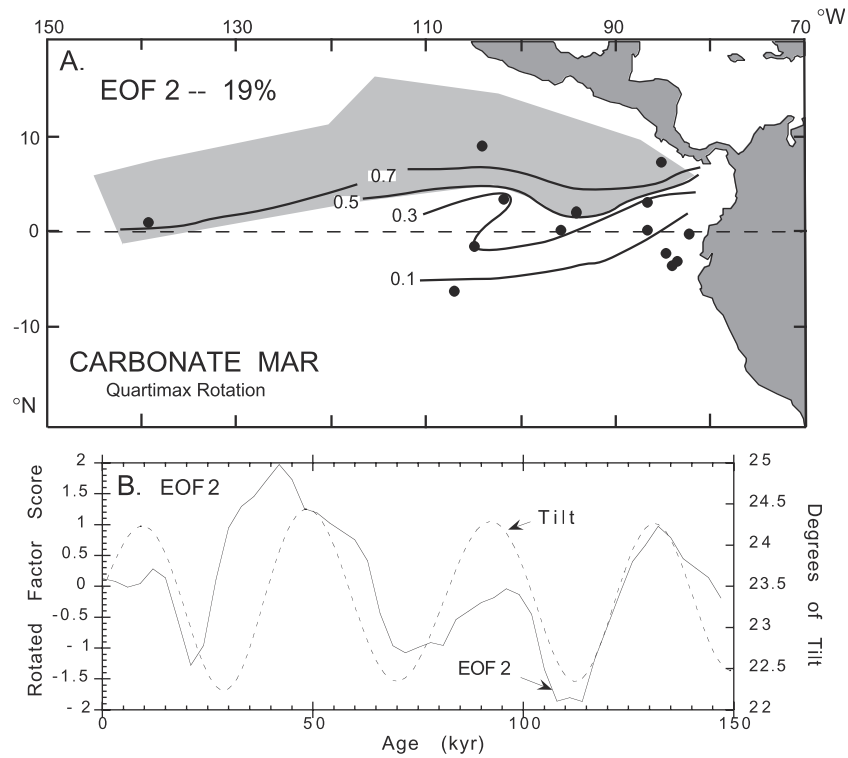
Figure 5. (a) Map pattern of factor loadings for EOF 2, which explains 19% of the variance in the CaCO3 MAR data set. This pattern has a northern source. (b) CaCO$_3$ MAR time series for EOF 2. The time series is coherent at >95% confidence interval with obliquity and is in phase.
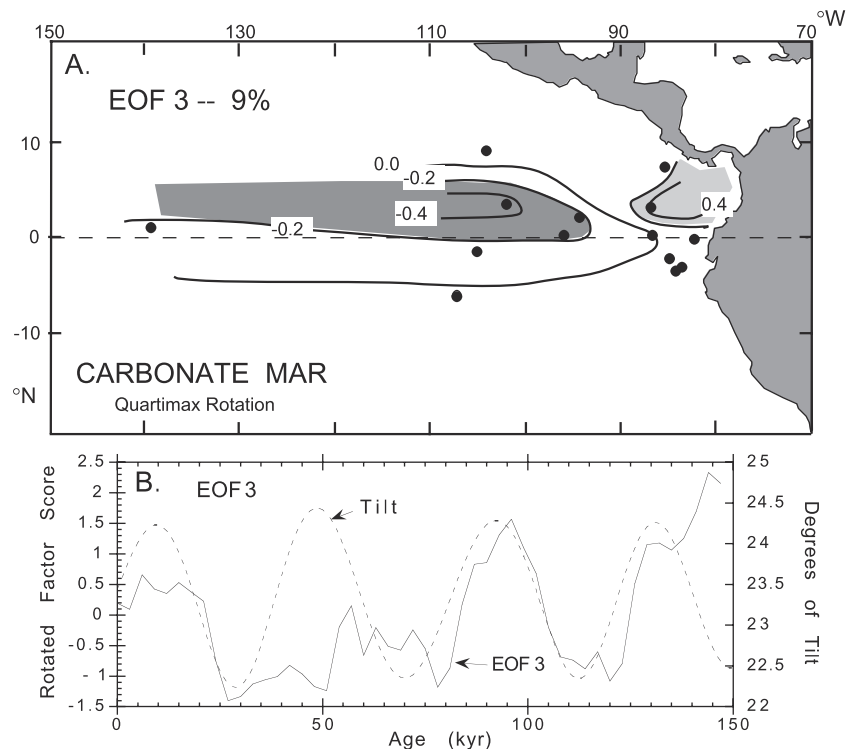

Figure 6. (a) Map pattern of factor loadings for EOF 3, which explains 9% of the variance in the CaCO$_3$ MAR data set. Note that strong positive loadings occur in the Panama Basin, while strong negative loadings occur to the west. This pattern appears centered on the North Equatorial Countercurrent. (b) CaCO$_3$ MAR time series for EOF 2. The time series is coherent at >95% confidence interval with obliquity and leads obliquity by 4–6 kyr.
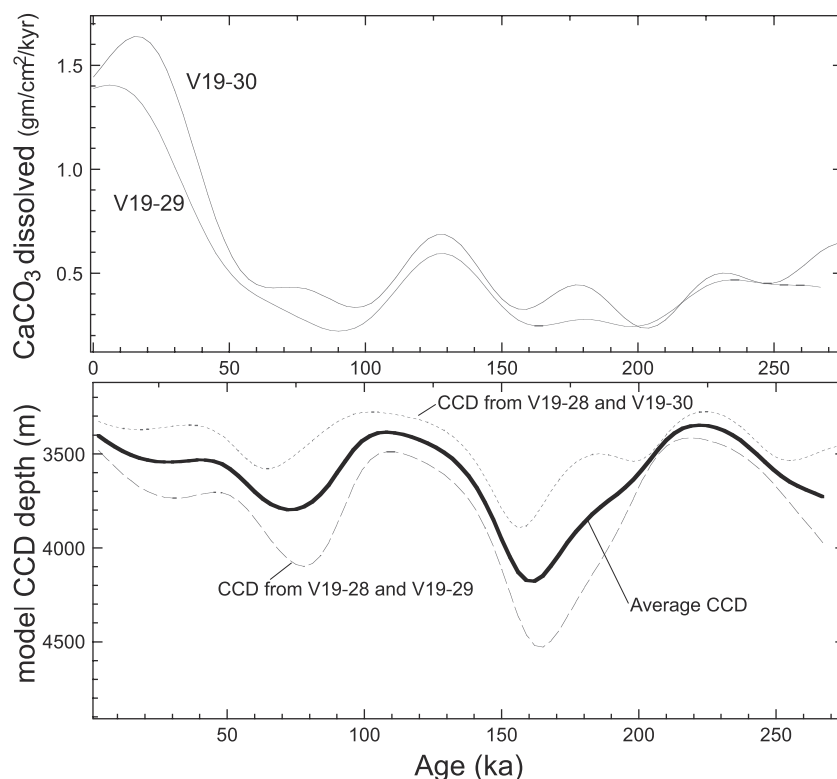
Figure 7. Model of (top) dissolution and (bottom) CCD in the Peru Basin using the cores V19-28, V19-29, and V19-30 (see Figure 3d). The cores are all located on the flank of the Carnegie Ridge within 160 km of each other. By assuming that V19-28, the shallowest core, is at the lysocline and that the flux of $CaCO_3$ is the same for all the cores, it is possible to calculate the rate of dissolution and the CCD for the Peru Basin. See text for details. See color version of this figure at back of this issue.

peak in MIS 2, while EOF 2 has its first peak at 50 ka, and EOF 3 has high MARs in MIS 6 (>125 ka). In each case, with minor variations, the C_{org} and opal MAR time series have the same shape as the $CaCO_3$ MAR time series. The sediment core with the least coherence among the three biogenic MAR time series is W8402-14GC, the westernmost and deepest core in the data set. This is also the core that probably has the highest dissolution signal.

7. EOF Distributions as Indicators of Surface Processes

[35] The regional distribution of the loadings for each EOF resemble surface water flow paths not deep flow, which is another line of evidence suggesting that the $CaCO_3$ MARs in the eastern Pacific are more highly controlled by productivity than dissolution.

7.1. EOF 1: the CaCO₃ Spike at the Last Glacial Maximum

[36] The map of EOF 1 loadings (Figure 4a) is similar to the flow path of the South Equatorial Current (Figure 2a). High loadings occur on both sides of the Carnegie Ridge in both the Panama Basin (Y69-71) and the Peru Basin (V19-28, V19-29, and V19-30) as well as on top of the ridge (V19-27). High loadings cross over the East Pacific Rise into the Pacific Basin proper to reach the westernmost core in this study, W8402-14GC. The lack of confinement to any particular basin is evidence of a surface source for this $CaCO_3$ pattern.

[37] We are confident that the EOF 1 spike is not an artifact of poor age control because the cores which are strongly loaded in

EOF 1 are some of the most extensively studied cores in the world. V19-29, for example, has a loading of 0.909 in EOF1. It is also the basis of the SPECMAP high-resolution chronology for 0–300 ka [*Martinson et al.*, 1987] and has a sedimentation rate that averages >6.5 cm/kyr for 0–150 ka.

[38] We are also confident that the EOF 1 spike is not a result of lateral transport of biogenic material from exposed shelves at the Last Glacial Maximum. *Loubere* [1999] suggested that the prominent C_{org} depositional event coincident with the EOF 1 $CaCO_3$ spike could perhaps be caused by lateral transport. However, shelf sediments contain too much aluminosilicates relative to the biogenic fraction to be a major fraction of the MIS 2 sediments.

[39] Published analyses of Peru margin sediments [*Reimers and Suess*, 1981], for example, indicate that the shelf and slope average ~5% C_{org}, and ~17% $CaCO_3$. If we assume a model shelf sediment composed of 5% C_{org}, 15% $CaCO_3$, 15% opal, and 65% aluminosilicates and assume that all the excess C_{org} arrived via lateral transport, we can calculate the amount of shelf sediment present and calculate the change in other sediment fractions. In Y69-71, if the excess C_{org} at the Last Glacial Maximum were shelf derived, $CaCO_3$ should be lower than the modern value of 61% (~55%), while the nonbiogenic content should be higher than the modern value of 12% (~19%). Opal percentage should be roughly the same. Instead, measured $CaCO_3$ is higher (~66%), and the nonbiogenic fraction is lower (~10%). Similar trends are observed in the other cores highly loaded in EOF 1.

[40] The pattern of EOF 1 (Figure 4a) suggests that either nutrient advection in the South Equatorial Current or dust carried by the southeast Trade Winds may be responsible for the elevated production. Nutrients are not fully utilized in the modern eastern
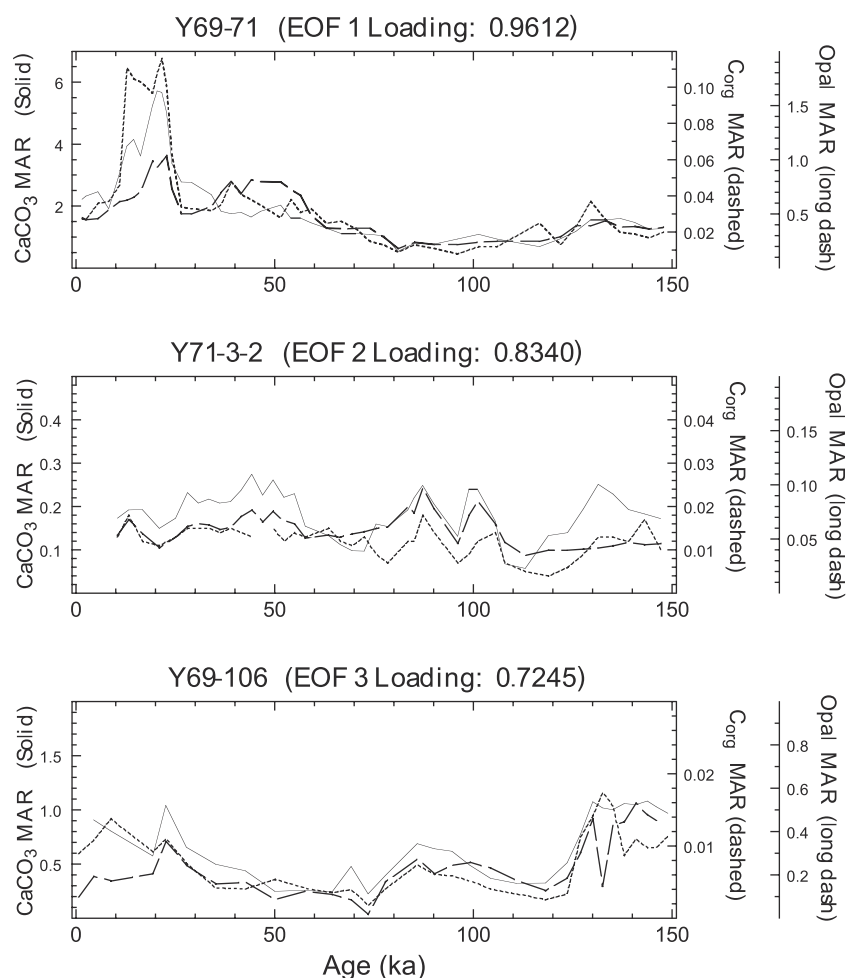
Figure 8. A comparison of $CaCO_3$, C_{org}, and opal MAR in EOF end-member cores (highly loaded in different ones of the $CaCO_3$ MAR EOF). All of these biogenic MAR are highly coherent, a condition that could only be caused by productivity not $CaCO_3$ dissolution caused by changes in deep water chemistry.

equatorial Pacific probably because a trace element limits production, e.g., iron [*Martin*, 1990; *Martin et al.*, 1994] or possibly zinc [*Morel et al.*, 1994]. Increased dust deposition should provide an additional flux of these trace metals into surface waters and cause higher productivity. We observe an increase in MAR of the nonbiogenic fraction (bulk MAR minus the biogenic MARs) at the EOF 1 spike in eastern Pacific cores (e.g., V19-28 and Y69-71) but do not observe high nonbiogenic MAR in the central Pacific (W8402A-14). However, W8402A-14 has so little nonbiogenic material that the apparent lack of detrital material could easily result from the crudity of this detrital estimate.

[41] Production stimulated by high dust should follow the pattern of the southeast trade winds, which bring dust to the eastern Pacific from South America. Modern aeolian deposition in the southeast trades based upon quartz [*Molina Cruz and Price*, 1977] or Al MAR [*Lyle*, 1992] forms a wedge outward from the Peru margin, extending in a lobe along the equator westward beyond 110°W. The pattern is similar to that of EOF 1.

[42] Aeolian deposition of either iron or zinc favors increased production by diatoms and better utilization of dissolved nitrates, causing a net drop in the ratio of $CaCO_3$ to C_{org} rain. The higher flux of C_{org} relative to $CaCO_3$ to the sediments could significantly lower the $CaCO_3$ MAR because of higher dissolution by C_{org} degradation. Because the existing evidence indicates that nitrogen

utilization did not improve [*Farrell et al.*, 1995a, 1995b], we favor the hypothesis that EOF 1 reflects surface currents.

[43] Nitrogen isotope evidence in the eastern Pacific [*Farrell et al.*, 1995a, 1995b] suggests that relative nitrate utilization dropped during MIS 2, even though primary productivity was higher. In other words, dissolved nitrate was supplied via upwelling or advection much faster than plankton could strip it from the euphotic zone, and plankton at the Last Glacial Maximum was even less efficient at using dissolved nitrate than the modern plankton assemblage. Perhaps the greater amount of nonutilized dissolved nitrates or other nutrients stimulated the $CaCO_3$-producing phytoplankton and led to significantly higher $CaCO_3$ production relative to the C_{org} production.

[44] Time series from our data and other longer records agree that the MIS 2 depositional spike represented by EOF 1 is the largest C_{org} burial event in the last 300 kyr [*Lyle et al.*, 1988; *Pedersen et al.*, 1991]. On the basis of one of the few really long MAR records (Ocean Drilling Program (ODP) Site 847, located near RC13-110 [*Murray et al.*, 1995]) the first $CaCO_3$ MAR event that approaches the MIS 2 event in strength occurs at ~350 ka in MIS 10. It becomes apparent that the MIS 2 $CaCO_3$ and C_{org} spike is a rare and important paleoceanographic event in the eastern tropical Pacific. The dynamics of the eastern tropical Pacific must have been significantly different at the Last Glacial

Maximum than during the average Late Pleistocene glacial period.

7.2. EOF 2: In Phase With Orbital Obliquity Cycles

[45] EOF 2 explains 19% of the total variance of the $CaCO_3$ MAR data set. It is a prominent time series in the northernmost cores but is also strong in the central Pacific core W8402A-14GC (Figure 5). From its distribution it is possible to argue that this EOF may have been caused by dissolution. The EOF has high loadings in both shallow and deep sediment cores, however. We conclude that this EOF also is a reflection of surface ocean processes. For example, the sediment core with the highest loading in EOF 2, Y71-3-2, was recovered on the Cocos Ridge at a water depth of 2164 mbsl.

[46] The time series shown in Figure 5b is highly coherent and in phase with the obliquity orbital cycle. This pattern suggests a direct and rapid link between EOF 2 and a component of insolation, also implying a surface process linked to high latitudes. Low-latitude insolation response to obliquity is small and out of phase with the tilt cycle, while high-latitude insolation response is large and in phase. The in-phase response with insolation is unusual with respect to paleoceanographic records. The paleoceanographic response from SPECMAP most closely in phase with obliquity [*Imbrie et al.*, 1992] still lags by 3–4 kyr, while minimum ice volume occurs 9–10 kyr after maximum obliquity.

[47] The in-phase response by EOF 2 to the obliquity cycle implies a strong and immediate tie to high-latitude insolation. Because maximum tilt of the Earth's orbit is the time of maximum high-latitude seasonality, it may also mark the maximum seasonal variability in the strength of eastern boundary currents. The appearance of EOF 2 in the north would link it most strongly to processes within the California Current system and its exchange of cold, nutrient-rich subarctic waters with the tropical eastern Pacific. We thus expect to find a similar response in the California Current system. We note from preliminary analysis of $CaCO_3$ records from the California Borderlands and the tip of Baja California that a strong obliquity response is apparent in the southern California Current region (Site 1012 (M. Lyle, unpublished data, 2001) and Y74-2-22 [*Lyle et al.*, 2000]). The weakness in the eastern boundary current hypothesis is the lack of a response within the Peru Current region.

[48] Another process that might cause EOF 2 is an interaction with the Intertropical Convergence Zone. Maximum high-latitude seasonality during maximum obliquity should drive the ITCZ through its maximum seasonal latitudinal range. The link between $CaCO_3$ production and movement of the ITCZ is unclear, however.

7.3. EOF 3: North Equatorial Countercurrent?

[49] EOF 3 is highly loaded on only two cores. It is positively loaded on the Panama Basin core Y69-106 and negatively loaded on RC10-62 from the East Pacific Rise. Both cores are from a latitude of 3°N, roughly at the southern edge of the average position of the North Equatorial countercurrent. Thus EOF 3 also has a distribution that appears to be surface driven.

[50] The antithetic response between Y69-106 and RC10-62 implies that the EOF may reflect an E-W cyclic process, either the strength of the North Equatorial Countercurrent or, conversely, strength of upwelling in the Panama Basin region. The seasonal upwelling along the central American coast is mainly driven by the occasional arrival of high pressure from Canada on the Caribbean side of the isthmus of Panama between December in March. Because of the topography of Central America these winds are funneled through three major passes at the Gulf of Tehuantepec, the Gulf of Papagayo, and the Gulf of Panama [*Hurd*, 1929; *Clarke*, 1988; *Legeckis*, 1988]. Upwelling would be strengthened if these winter storms penetrated from the Caribbean more frequently, as should occur when winter insolation in the high latitudes is lowest.

Such a scenario would fit with the coherent behavior between EOF 3 and orbital obliquity because high obliquity marks maximum seasonality and minimum winter insolation.

8. Comparisons to Other Eastern Pacific Studies

[51] Other studies have searched for spatial patterns in the eastern Pacific, and the types of patterns they have found depend on timescale and site distribution [*Hagelberg et al.*, 1995; *Pisias and Mix*, 1997; *Mix et al.*, 1999]. *Hagelberg et al.* [1995] studied the longest time series, from 0 to 6 Ma, and found two EOF patterns that were responsible for 77% of the $CaCO_3$ MAR/$CaCO_3$ percentage data. One EOF was associated with equatorial upwelling and is coherent with insolation, while a second EOF appears to reflect closure of the Panama Gateway and is only comprehensible in the percentage data. The first EOF can be subdivided by its spectral character, and the spectral band with periods >45 kyr has a spatial pattern similar to EOF 1 of this study. Because of the low-frequency character of EOF 1 of this study we expected equivalence with the low-frequency band. The second EOF of *Hagelberg et al.* [1995] only seems to have a geographic pattern in the percentage data and shows a west-east shift in carbonate percentages from low to high at ~3.5 Ma, perhaps caused by the closure of the Panama Gateway [*Farrell et al.*, 1995b].

[52] *Pisias and Mix* [1997] used eight cores in common with this study. They reported on spatial variability in the eastern Pacific of radiolarian-derived sea surface temperatures and extracted three EOF from that data set. Of these, there is a similarity between EOF 1 of this study and EOF 1 of *Pisias and Mix* [1997]. Cold sea surface temperatures (SST) in the eastern and equatorial regions in *Pisias and Mix* [1997] EOF 1 is equivalent to the high carbonate in this study's EOF 1. The time series of the EOF are similar except in MIS 2, where the amplitude of the $CaCO_3$ spike is very much greater than the SST drop noted in the temperature data.

[53] *Mix et al.* [1999] also show a similar geographic pattern to this study's EOF 1 in their Last Glacial Maximum estimate of SST through a new foraminiferal faunal SST estimate. The spatial coherence between SST and $CaCO_3$ MAR is additional evidence that EOF 1 is a production signal, probably associated with a cold water plankton community (at least for the equatorial region). Similarly, highest $CaCO_3$ MAR at Site 846 occurred during an interval of the coldest temperatures between 250 and 500 ka [*Emeis et al.*, 1995]. The association between high $CaCO_3$ MAR and relatively low temperature is not observed in the Milankovitch frequency bands at Site 846, however. We expect that the link between plankton community structure and $CaCO_3$ burial may be relatively complex and meriting further study.

[54] The major point of disagreement between this study and with previous work is with the study of *Loubere* [1999]. He used assemblages of benthic foraminifera to estimate that MIS 2 had ~25% lower productivity than modern conditions. He used at least some of the same cores that we used in this study (Y69-71 and V19-28) where both $CaCO_3$ MAR and C_{org} spikes are prominent in MIS 2. He has suggested that the C_{org} spike may be derived by better preservation during MIS 2 or, as discussed earlier, is the result of lateral transport of sediment from nearby continental shelves. We reiterate our conclusion that the preserved sediment signal is not indicative of lateral transport from a shelf source. We expect a relatively high detrital and low $CaCO_3$ content from shelf sediments as well as high C_{org}. This is not reflected in the records we have over the MIS 2 interval. Instead, where the MIS 2 $CaCO_3$ spike exists, we observe higher $CaCO_3$ deposition than modern conditions throughout the water column from 1370 (V19-27) to 3157 m (V19-29).

[55] Without an increase in carbon rain from the surface waters, it is difficult to produce a $CaCO_3$ MAR spike at MIS 2 by processes that would also preserve C_{org}. If the entire water column went

anoxic to the point that seawater sulfate was reduced, it is possible to increase preservation of both $CaCO_3$ and C_{org}. However, benthic foraminifera should not survive such an event. In addition, the size of the event would have had to be huge. To cover cores where the MIS 2 event has been identified, the anoxic region would have to cover the entire northern Nazca Plate as well as the Panama Basin from ~1 km water depth to >3 km. An anoxic event of this size should be obvious in a variety of other sediment indices and it is not apparent. We suspect instead that the paleoproductivity estimate of *Loubere and Fariduddin* [1999] is not as robust as they claim, at least for the pelagic environment. The lack of a signal at MIS 2 in assemblages of benthic foraminifera in the eastern tropical Pacific is still a problem that must be addressed by future work.

9. Conclusions

[56] There is no simple pattern of $CaCO_3$ burial in the eastern tropical Pacific region for the last 150 kyr. Cores from distinct subregions have distinctive patterns of $CaCO_3$ weight percent, partly because of variability in $CaCO_3$ production and burial but also because different regions of the eastern tropical Pacific have variable deposition of clays and opal. Converting to burial flux ($CaCO_3$ MAR) eliminates the dilution problems, but the resulting patterns of $CaCO_3$ MAR are still complex. For this reason, we employed EOF analysis to group our data into independent modes of variability. We conclude that all of the EOF modes we discovered are driven by variability of $CaCO_3$ production not dissolution.

[57] The most important mode of variability (EOF 1) explained slightly more than half of the variance in our data set and is represented by a spike of $CaCO_3$ MAR during MIS 2. This spike is coincident with the well-known productivity spike at that time [*Pedersen*, 1983; *Lyle et al.*, 1988; *Pedersen et al.*, 1991]. The $CaCO_3$ MAR spike is the largest event in the last 300 kyr. A previous period of equivalent $CaCO_3$ MAR can only be found at ~350 ka at ODP Site 847 [*Murray et al.*, 1995]. We have concluded

that EOF 1 represents an unusual $CaCO_3$ production and C_{org} burial event not related to the typical insolation cycles. Because the Last Glacial Maximum is unusual, MIS 2 probably should not be used as the "type" glacial interval in the eastern tropical Pacific Ocean.

[58] EOF 2, on the contrary, does have strong coherence with the obliquity cycle. Because it is coherent and in phase with obliquity, we suspect a strong high-latitude influence as the origin of the mode of variability. The strength of this EOF does not depend upon depth, and the $CaCO_3$ MAR is also coherent with C_{org} and opal MARs, which has led us to conclude that this EOF also records variability in production not dissolution. Because EOF 2 is strongest in the north of our study, we also suspect a link to the North Pacific, possibly through the California Current system. Alternately, shifts of the Intertropical Convergence Zone driven by obliquity could cause this signal. Further work to compare California Current sediment cores with those of the eastern tropical Pacific Ocean will help to clarify these processes. EOF 3 also is coherent with obliquity, but its regional pattern suggests a link with the North Equatorial Countercurrent. Conversely, it could be related to the strength of winds across the isthmus of Panama.

[59] Finally, it is important to note that $CaCO_3$ stratigraphy should be applied with care in the eastern tropical Pacific Ocean especially for high-resolution work. While general trends are similar to the central Pacific, details are not. Peak-to-peak correlations can lead to significant errors in the resultant age model for the late Pleistocene. With some care and an eye to the regional variation, however, $CaCO_3$ content is sufficiently variable in time to provide good stratigraphic control.

References

Archer, D. E., Equatorial Pacific calcite preservation cycles: Production or dissolution, *Paleoceanography, 6*, 561–571, 1991.

Arrhenius, G. O. S., Sediment cores from the east Pacific, *Rep. Swed. Deep Sea Exped. 1947–1948, 5*, 1–228, 1952.

Berelson, W. M., D. E. Hammond, J. McManus, and T. E. Kilgore, Dissolution kinetics of calcium carbonate in equatorial Pacific sediments, *Global Biogeochem. Cycles, 8*, 219–235, 1994.

Berger, W. H., Sedimentation of planktonic foraminifera, *Mar. Geol., 11*, 325–358, 1971.

Berger, W. H., Pacific carbonate cycles revisited: Arguments for and against productivity control., in *Centenary of Japanese Micropaleontology*, edited by K. Ishizaki and T. Saito, pp. 15–25, Terra Sci., Tokyo, 1992.

Berger, W. H., M.-C. Bonneau, and F. L. Parker, Foraminifera on the deep-sea floor: Lysocline and dissolution rate, *Oceanol. Acta, 5*, 249–258, 1982.

Broecker, W. S., Calcite accumulation rates and glacial to interglacial changes in oceanic mixing, in *Late Cenozoic Glacial Ages*, edited by K. K. Turekian, pp. 239–265, Yale Univ. Press, New Haven, Conn., 1971.

Broecker, W. S., Ocean chemistry during glacial time, *Geochim. Cosmochim. Acta, 46*, 1689–1705, 1982.

Broecker, W. S., and T. Takahashi, The relationship between lysocline depth and in situ car-

bonate ion concentration, *Deep Sea Res., 25*, 65–95, 1978.

Clarke, A. J., Inertial wind path and sea surface temperature patterns near the Gulf of Tehuantepec and Gulf of Papagayo, *J. Geophys. Res, 93*, 15,491–15,501, 1988.

Dymond, J., Geochemistry of Nazca Plate surface sediments: An evaluation of hydrothermal, biogenic, detrital, and hydrogenous sources, in *Nazca Plate: Crustal Formation and Andean Convergence*, edited by L. Kulm et al., *Mem. Geol. Soc. Am., 154*, 269–294, 1981.

Emeis, K.-C., H. Doose, A. Mix, and D. Schulz-Bull, Alkenone sea-surface temperatures and carbon burial at Site 846 (eastern equatorial Pacific Ocean): The last 1.3 M.Y., *Proc. Ocean Drill. Program Sci. Results, 138*, 605–613, 1995.

Farrell, J. W., and W. L. Prell, Climatic change and $CaCO_3$ preservation: An 800,000 year bathymetric reconstruction from the central equatorial Pacific Ocean, *Paleoceanography, 4*, 447–467, 1989.

Farrell, J. W., T. F. Pedersen, S. E. Calvert, and B. Nielson, Glacial-interglacial changes in nutrient utilization in the equatorial Pacific Ocean, *Nature, 377*, 514–517, 1995a.

Farrell, J. W., I. Raffi, T. R. Janecek, D. W. Murray, M. Levitan, K. A. Dadey, K.-C. Emeis, M. Lyle, J.-A. Flores, and S. Hovan, Late Neogene sedimentation patterns in the

eastern equatorial Pacific Ocean, *Proc. Ocean Drill. Program Sci. Results, 138*, 717–756, 1995b.

Grötsch, J., G. Wu, and W. H. Berger, Carbonate cycles in the Pacific: Reconstruction of Saturation fluctuations, in *Cycles and Events in Stratigraphy*, edited by G. Einsele, W. Ricken, and A. Seilacher, pp. 111–124, Springer-Verlag, New York, 1991.

Gordon, A. L., Spreading of Antarctic Bottom waters, II, in *Studies in Physical Oceanography: A tribute to Georg Wüst on his 80th birthday*, vol. 2, edited by A. L. Gordon, pp. 1–19, Gordon and Breach, Newark, N. J., 1972.

Hagelberg, T. K., N. G. Pisias, L. A. Mayer, N. J. Shackleton, and A. C. Mix, Spatial and temporal variability of late Neogene equatorial Pacific Carbonate: Leg 138, in *Proc. Ocean Drill. Program Sci. Results,, 138*, 321–337, 1995.

Honjo, S., J. Dymond, R. Collier, and S. J. Manganini, Export production of particles to the interior of the equatorial Pacific Ocean during the 1992 EqPac experiment, *Deep Sea Res., 42*, 831–870, 1995.

Hurd, W. E., Northers of the Gulf of Tehuantepec, *Mon. Weather Rev., 57*, 192–194, 1929.

Imbrie, J., J. D. Hays, D. G. Martinson, A. McIntyre, A. C. Mix, J. J. Morley, N. G. Pisias, W. L. Prell, and N. J. Shackleton, The orbital theory of Pleistocene climate: Support from a revised chronology of the marine δ¹⁸O record,

in *Milankovitch and Climate, Part I*, edited by A. L. Berger, pp. 269–305, D. Reidel, Norwell, Mass., 1984.

Imbrie, J., et al., On the structure and origin of major glaciation cycles, 1, Linear responses to Milankovitch forcing, *Paleoceanography*, 7, 701–739, 1992.

Jahnke, R. A., D. B. Craven, D. C. McCorkle, and C. E. Reimers, CaCO$_3$ dissolution in California continental margin sediments: The influence of organic matter remineralization, *Geochim. Cosmochim. Acta*, 61, 3587–3604, 1997.

Le, J., A. C. Mix, and N. J. Shackleton, Late Quaternary paleoceanography in the eastern equatorial Pacific Ocean from planktonic foraminifers: A high-resolution record from Site 846, *Proc. Ocean Drill. Program Sci. Results*, 138, 675–693, 1995.

Legeckis, R., Upwelling off the Gulfs of Panama and Papagayo in the tropical Pacific during March 1985, *J. Geophys. Res*, 93, 15,485–15,489, 1988.

Lonsdale, P., Abyssal circulation of the southeastern Pacific and some geological implications, *J. Geophys. Res.*, 81, 1163–1176, 1976.

Loubere, P., A multiproxy reconstruction of biological productivity and oceanography in the eastern equatorial Pacific for the past 30,000 years, *Mar. Micropaleontol.*, 37, 173–198, 1999.

Loubere, P., and M. Fariduddin, Quantitative estimation of global patterns of surface ocean biolobical productivity and its seasonal variation on timescales from centuries to millennia, *Global Biogeochem. Cycles*, 13, 115–135, 1999.

Lyle, M., Composition maps of surface sediments of the eastern tropical Pacific Ocean, *Proc. Ocean Drill. Program Initial Rep.*, 138, 101–115, 1992.

Lyle, M., D. Murray, B. Finney, J. Dymond, J. Robbins, and K. Brooksforce, The record of late Pleistocene biogenic sedimentation in the eastern tropical Pacific Ocean, *Paleoceanography*, 3, 39–59, 1988.

Lyle, M., K. Dadey, and J. Farrell, The late Miocene (11–8 Ma) eastern Pacific carbonate crash: Evidence for reorganization of deep water circulation by the closure of the Panama Gateway, *Proc. Ocean Drill. Program Sci. Results*, 138, 821–837, 1995.

Lyle, M., A. Mix, C. Ravelo, D. Andreasen, L. Heusser, and A. Olivarez, Millennial-scale CaCO$_3$ and C-org events along the northern and central California margin: Stratigraphy and origins, *Proc. Ocean Drill. Program Sci. Results*, 167, 163–182, 2000.

Mantyla, A. W., On the potential temperature in the abyssal Pacific Ocean, *J. Mar. Res.*, 33, 341–353, 1975.

Martin, J. H., Glacial-interglacial CO$_2$ change: The iron hypothesis, *Paleoceanography*, 5, 1–15, 1990.

Martin, J. H., et al., Testing the iron hypothesis in ecosystems of the equatorial Pacific Ocean, *Nature*, 371, 123–129, 1994.

Martinson, D. G., N. G. Pisias, J. D. Hays, J. Imbrie, T. C. Moore Jr., and N. J. Shackleton, Age dating and the orbital theory of the ice ages: Development of a high-resolution 0–300,000-year chronostratigraphy, *Quat. Res.*, 27, 1–29, 1987.

Mix, A. C., A. E. Morey, N. G. Pisias, and S. W. Hostetler, Foraminiferal faunal estimates of paleotemperature: Circumventing the no-analog problem yields cool ice age tropics, *Paleoceanography*, 14, 350–359, 1999.

Molina Cruz, A., Paleo-oceanography of the subtropical southeastern Pacific during the late Quaternary: A study of radiolaria, opal, and quartz contents of deep-sea sediments, M.Sc. thesis, Oreg. State Univ., Corvallis, 1976.

Molina Cruz, A., and P. Price, Distribution of opal and quartz in the ocean-floor of the subtropical southeastern Pacific, *Geology*, 5, 81–84, 1977.

Morel, F. M. M., J. R. Reinfelder, S. B. Roberts, C. P. Chamberlain, J. G. Lee, and D. Yee, Zinc and carbon co-limitation of marine plankton, *Nature*, 369, 740–742, 1994.

Mortlock, R. A., and P. N. Froelich, A simple method for the rapid determination of biogenic opal in pelagic marine sediments, *Deep Sea Research*, 36, 1415–1426, 1989.

Murray, D. W., Spatial and temporal variations in sediment accumulation in the central tropical Pacific, Ph.D. thesis, 343 pp., Oreg. State Univ., Corvallis, 1987.

Murray, D. W., J. W. Farrell, and V. McKenna, Biogenic sedimentation at Site 847, eastern equatorial Pacific Ocean during the last 3 m.y., *Proc. Ocean Drill. Program Sci. Results*, 138, 821–839, 1995.

Paytan, A., M. Kastner, and F. P. Chavez, Glacial to interglacial fluctuations in productivity in the equatorial Pacific as indicated by marine barite, *Science*, 274, 1355–1357, 1996.

Pedersen, T. F., Increased productivity in the eastern equatorial Pacific during the Last Glacial Maximum (19000 to 14000 yr B.P.), *Geology*, 11, 16–19, 1983.

Pedersen, T. F., B. Nielsen, and M. Pickering, Timing of late Quaternary productivity pulses in the Panama Basin and implications for atmospheric CO$_2$, *Paleoceanography*, 6, 657–667, 1991.

Pisias, N., Model of late Pleistocene-Holocene variations in rate of sediment accumulation: Panama Basin, eastern equatorial Pacific, MSc. thesis, 77 pp., Oreg. State Univ., Corvallis, 1974.

Pisias, N., and A. Mix, Spatial and temporal oceanographic variability of the eastern equatorial Pacific during the late Pleistocene: Evidence from radiolaria microfossils, *Paleoceanography*, 12, 381–393, 1997.

Pytkowicz, R. M., Chemical solution of calcium carbonate in sea water, *Am. Zool.*, 9, 673–679, 1969.

Reimers, C. E., and E. Suess, Spatial and temporal patterns of organic matter accumulation on the Peru continental margin, in *Coastal Upwelling: Its Sediment Record,* part B, *Sedimentary Records of Coastal Upwelling*, edited by J. Thiede, and E. Suess, pp. 311–345, Plenum, New York, 1981.

Sarnthein, M., K. Winn, J.-C. Duplessy, and M. R. Fontugne, Global variations of surface ocean productivity in low and mid latitudes: Influence on CO$_2$ reservoirs of the deep ocean and atmosphere during the last 21,000 years, *Paleoceanography*, 3, 361–399, 1988.

Snoeckx, H., and D. K. Rea, Late Quaternary CaCO$_3$ stratigraphy of the eastern equatorial Pacific, *Paleoceanography*, 9, 341–351, 1994.

Tsuchiya, M., and L. D. Talley, A Pacific hydrographic section at 88°W: Water-property distribution, *J. Geophys. Res*, 103, 12,899–12,918, 1998.

Weber, M. E., M. Wiedicke, V. Riech, and H. Erlenkeuser, Carbonate preservation history in the Peru Basin: Paleoceanographic implications, *Paleoceanography*, 10, 775–800, 1995.

Weliky, K., E. Suess, C. A. Ungerer, P. Müller, and K. Fischer, Problems with accurate carbon measurements in marine sediments and particulate matter in seawater: A new approach, *Limnol. Oceanogr.*, 28, 1252–1259, 1983.

Wyrtki, K., Equatorial currents in the Pacific 1950 to 1970 and their relations to the trade winds, *J. Phys. Oceanol.*, 4, 372–380, 1974.

————————

M. Lyle, Center for Geophysical Investigation of the Shallow Subsurface, Boise State University, Boise, ID 83725-1536, USA. (mlyle@cgiss.boisestate.edu)

A. Mix and N. Pisias, College of Ocean and Atmospheric Sciences, Oregon State University, Corvallis, OR 97331-5503, USA.
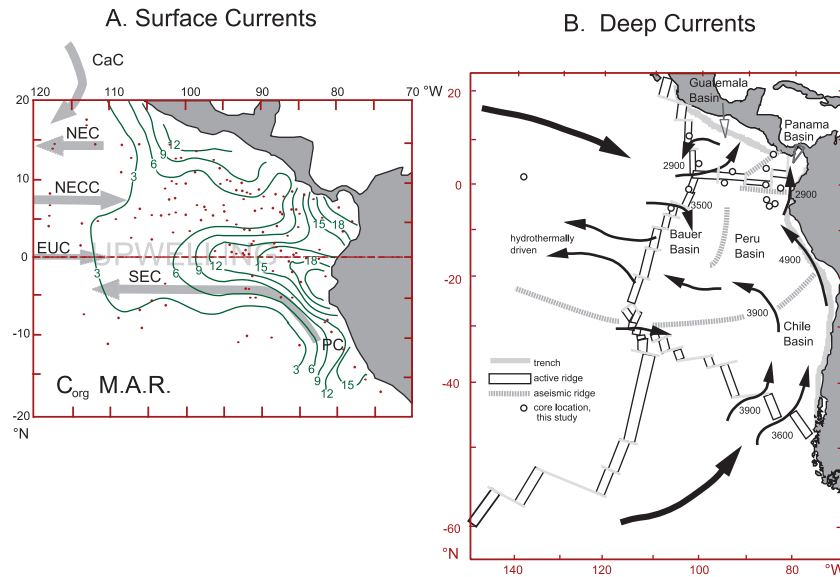
A. Surface Currents

B. Deep Currents

Figure 2. (a) Surface currents of the eastern tropical Pacific Ocean superimposed upon C_{org} mass accumulation rate (MAR) from *Lyle* [1992]. C_{org} MAR is a semiquantitative measure of productivity in the water column. CaC, California Current; EUC, Equatorial Undercurrent; NEC, North Equatorial Current; NECC, North Equatorial Countercurrent; SEC, South Equatorial Current. (b) Deep water flow paths in the eastern Pacific, based upon *Lonsdale* [1976] with additions from *Dymond* [1981] and *Lyle* [1992].
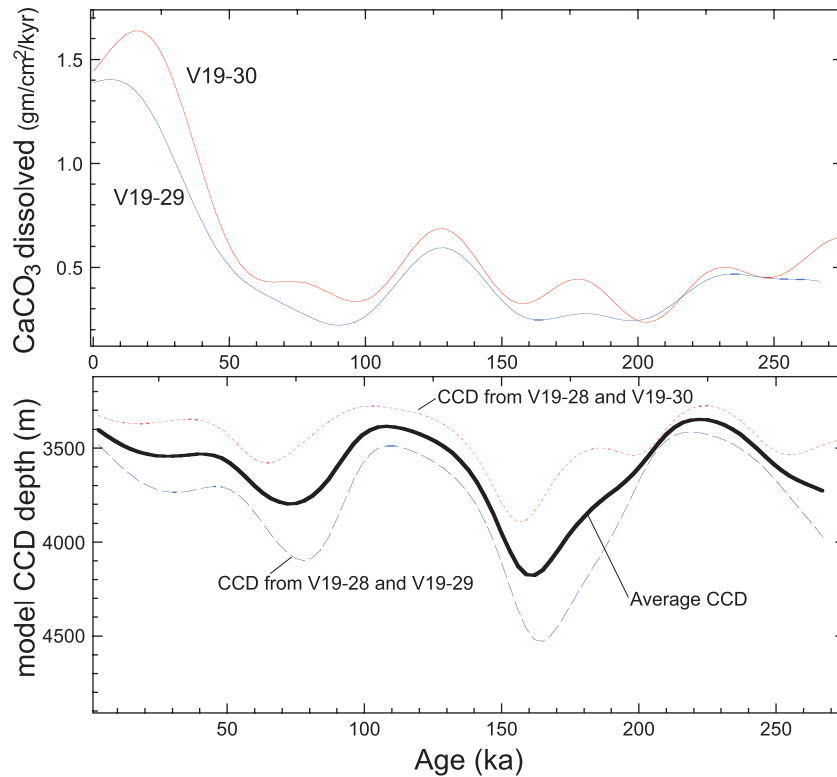

Figure 7. Model of (top) dissolution and (bottom) CCD in the Peru Basin using the cores V19-28, V19-29, and V19-30 (see Figure 3d). The cores are all located on the flank of the Carnegie Ridge within 160 km of each other. By assuming that V19-28, the shallowest core, is at the lysocline and that the flux of $CaCO_3$ is the same for all the cores, it is possible to calculate the rate of dissolution and the CCD for the Peru Basin. See text for details.